

ISOCAM Mid-Infrared Imaging of the Quiescent Spiral Galaxy NGC 7331¹

Beverly J. Smith²

IPAC/Caltech, MS 100-22, Pasadena CA 91125

To appear in the *Astrophysical Journal*

Received _____; accepted _____

¹Based on observations made with ISO, an ESA project with instruments funded by ESA Member States and with the participation of ISAS and NASA.

²Now at CASA, University of Colorado, Box 389, Boulder CO 80309

ABSTRACT

Using the mid-infrared camera (ISOCAM) on the Infrared Space Observatory (ISO), the Sb LINER galaxy NGC 7331 has been imaged in two broadband and four narrowband filters between 6.75 and 15 μm . These maps show a prominent circumnuclear ring of radius $0\farcs25 \times 0\farcs75$ (1.1 \times 3.3 kpc) encircling an extended central source. The 7.7 and 11.3 μm dust emission features are strong in this galaxy, contributing $\sim 1/3$ of the total IRAS 12 μm broadband flux from this galaxy. In contrast to starburst galaxies, the 15 μm continuum is weak in NGC 7331. The mid-infrared spectrum does not vary dramatically with position in this quiescent galaxy, showing neither large-scale destruction of the carriers of the emission bands or a large increase in the 15 μm continuum in the star forming ring. In the bulge, there is some enhancement of the 6.75 μm flux, probably because of contributions from photospheric light, however, the 11.3 μm dust feature is also seen, showing additional emission from interstellar or circumstellar dust.

Subject headings: Galaxies: Individual (NGC 7331) – Galaxies: ISM – Infrared: Galaxies

1. Introduction

The standard picture of interstellar dust has changed dramatically in recent years, with the realization that molecule-sized dust grains transiently heated to very high temperatures may contribute significantly to the infrared emission from the interstellar medium (Sellgren 1984; Boulanger & Perault 1988). The characteristic set of mid-infrared emission features at 3.3, 6.2, 7.7, 8.6, and 11.3 μm , commonly known as the Unidentified Infrared Bands (UIBs), are likely caused by very small grains. Polycyclic aromatic hydrocarbons (PAHs) are most often cited as the origin of these features (Léger & Puget 1984); other possible carriers are hydrogenated amorphous carbons (Borghesi, Bussoletti, & Colangeli 1987), quenched carbonaceous compounds (Sakata et al. 1984), and coal grains (Papoula et al. 1989). Before the advent of the Infrared Space Observatory (ISO; Kessler et al. 1996), ground-based spectroscopy revealed the presence of UIBs in luminous starburst galaxies (e.g., Roche et al. 1991), however, the strength of these features in lower luminosity galaxies was unknown. IRAS broadband studies showed an increase in the 12 μm /60 μm ratio with decreasing far-infrared luminosity L_{FIR} (Smith et al. 1987; Helou et al. 1991). This suggests that small grains dominate the emission in the IRAS 12 μm bandpass and are systematically destroyed in environments with strong UV radiation fields, and so the UIB features should be strong in lower luminosity galaxies. This conclusion, however, could not be verified spectroscopically.

The higher sensitivity of ISO has now made it possible to study very small grains in lower luminosity galaxies as well as a variety of environments in starburst galaxies. With the ISO Camera (ISOCAM; Cesarsky et al. 1996), spatial as well as spectral information is obtained, providing important clues to the distribution of small grains within galaxies. For example, imaging spectroscopy of the starburst Antennae galaxies with the Circular Variable Filter (CVF) mode of CAM showed differences in the mid-infrared spectra of

starburst vs more quiescent regions (Vigroux et al. 1996); areas with large populations of OB stars have more emission in the $15 \mu\text{m}$ continuum relative to the UIBs. For fainter galaxies, where CVF imaging is not feasible, the strength and distribution of the UIBs can be estimated indirectly, using broadband ISO mid-infrared colors (e.g., Sauvage et al. 1996; Helou et al. 1996).

The narrowband ISOCAM filters provide a better method of tracing very small grains in fainter galaxies, because they isolate the UIB lines and give a better measure of the continuum than broadband filters. In this paper, both broad- and narrow-band ISOCAM mid-infrared images of the Sb galaxy NGC 7331 are presented. NGC 7331 is a nearby (15 Mpc for $H_0 = 75 \text{ km s}^{-1} \text{ Mpc}^{-1}$) relatively undisturbed spiral galaxy (see Figure 1 (Plate L1)). It has $L_{FIR} \sim 2 \times 10^{10} L_\odot$ (Rice et al. 1988), similar to that of the Milky Way (Cox, Krügel, & Mezger 1986), a weak LINER-like nucleus (Keel 1983a), and a post-starburst population in the bulge (Ohyama & Taniguchi 1996). Radio continuum (Cowan et al. 1994) and $\text{H}\alpha + [\text{N II}]$ imaging (Keel 1983b; Pogge 1989) show a faint nucleus surrounded by weak diffuse bulge emission, implying a low star formation rate in the bulge. The bulge is encircled by prominent spiral arms in a ring-like structure. The bulge appears to be depleted of both HI (Bosma 1981) and molecular gas (von Linden et al. 1996; Tosaki & Shioya 1997), compared to the surrounding spiral arms. In the mid-and far-infrared, IRAS could not resolve the bulge from the arms; this is also the case for Kuiper Airborne Observatory far-infrared maps (Smith & Harvey 1996). The new ISO images provide not just higher spatial resolution and sensitivity than IRAS, but also spectral information. By imaging in narrowband filters, we are able to isolate emission in the dust features from continuum emission, and directly detect the UIB features in a non-starburst galaxy and determine their spatial distribution.

2. Observations and Data Reduction

The ISO observations were made on 1996 December 25, 26, and 30 using the 32×32 element ISOCAM array on the 0.6m ISO telescope. Six different filters were used: the broadband LW2 ($\lambda_0 = 6.75 \mu\text{m}$; $\Delta\lambda = 3.5 \mu\text{m}$) and LW3 ($\lambda_0 = 15 \mu\text{m}$; $\Delta\lambda = 6 \mu\text{m}$) filters and the narrowband LW6 ($\lambda_0 = 7.75 \mu\text{m}$; $\Delta\lambda = 1.5 \mu\text{m}$), LW7 ($\lambda_0 = 9.62 \mu\text{m}$; $\Delta\lambda = 2.2 \mu\text{m}$), LW8 ($\lambda_0 = 11.4 \mu\text{m}$; $\Delta\lambda = 1.3 \mu\text{m}$), and LW9 ($\lambda_0 = 15 \mu\text{m}$; $\Delta\lambda = 2 \mu\text{m}$) filters. The observed region is marked in Figure 1 (Plate L1). A 7×2 mosaic was made, using $3''$ pixels and an overlap of $45''$, giving a total field of view of $135'' \times 350''$. The major axis of the raster is aligned at a position angle of 80° , perpendicular to the major axis of the galaxy, to give sufficient off-galaxy sky to determine the background. Along the major axis of the galaxy, the coverage is sufficient to map the inner spiral arms of NGC 7331. Twelve five second exposures were made per raster position. For stabilization, before these observations a series of additional exposures were made, with counts ranging from 19 to 67.

After standard ISOCAM pipeline reduction, additional data reduction was accomplished using the CAM Interactive Analysis (CIA) software³ as well as software developed at IPAC. Deglitching was done automatically with the Multi-resolution Median Transform routine (Starck et al. 1995) and by hand with an interactive deglitching routine developed at IPAC, and vignetted pixels on the edges of the array were masked. Transient effects (Cesarsky et al. 1996) were corrected for using the latest version of the IPAC simple analytic transient removal software (Seibbenmorgen et al. 1997), which models both upwards and downwards transients. Flat fields were created using the median of the off-galaxy raster positions, and the library darks were used. After dark subtraction and flat fielding, the individual frames

³CIA is a joint development by the ESA Astrophysics Division and the ISOCAM Consortium led by the ISOCAM PI, C. Cesarsky, Direction des Sciences de la Matière, C.E.A., France.

were mosaicked and the sky subtracted, and the standard ISO library calibration factors were used. The calibration uncertainty is estimated to be $\leq 30\%$.

3. The Mid-Infrared Morphology

The six ISOCAM images are presented in Figures 2a to 2f (Plates L2a-f). A prominent ring is seen at all wavelengths, with a diameter of $0\farcm5 \times 1\farcm5$ (2.2 kpc \times 6.5 kpc). Inside this ring, a central source is visible. This source is resolved with respect to the ISO beam, with an observed FWHM size of $\sim 7'' - 9''$ along the major axis. Outside of the ring, secondary arcs are visible. For comparison, the red continuum 6435\AA narrowband image and the H α +[N II] map from Pogge (1989) are shown in Figures 3a and 3b (Plates L3a and L3b), along with the LW3 image (Figure 3c) (Plate L3c). In Figures 3d, 3e, and 3f (Plates L3d-f), the H α +[N II] map, the radio continuum map of Cowan et al. (1994), and the CO map of Tosaki & Shioya (1997), respectively, are overlaid on the LW3 map. These maps show a good correspondence between the mid-infrared structure and features seen at other wavelengths. There is a good match between the mid-infrared and H α +[N II] peaks (Figure 3d), however, the ring is much more prominent in the mid-infrared than in H α +[N II]. This is particularly true for the western side of the ring which is quite faint in the optical, probably because of high extinction in this region. In the radio continuum and CO maps as well as in the mid-infrared, these obscured H II regions are bright. The optically-prominent H II regions in the spiral arms outside of the ring are also present in the mid-infrared maps, but at much lower flux levels (see Figures 2, 3c, and 3d).

Although the NGC 7331 mid-infrared morphology resembles that seen in the Sb galaxy M31 by IRAS (Habing et al. 1984), there are some important differences between these galaxies. M31 is an even more quiescent galaxy than NGC 7331, with $L_{FIR} \sim 25$ times lower than NGC 7331 and a much colder F₆₀/F₁₀₀ color temperature (Rice et al. 1988).

Furthermore, the M31 ring is ~ 3 times larger than the NGC 7331 ring. NGC 7331 may also resemble the Milky Way in mid-infrared morphology. The Galaxy is believed to contain a molecular ring of radius ~ 5 – 6 kpc (Sanders, Solomon, & Scoville 1984, Bronfman et al. 1988), which may also have an infrared counterpart (Sodroski et al. 1997). IRAS maps show a central mid-infrared peak in the Milky Way with a similar size scale as the source in NGC 7331 (Gautier et al. 1984).

4. The Mid-Infrared Spectral Energy Distribution

The mid-infrared spectrum of NGC 7331 is given in Figure 4a. The LW6 ($7.75\ \mu\text{m}$) and LW8 ($11.4\ \mu\text{m}$) fluxes are enhanced relative to the fluxes in the narrowband continuum filters LW7 ($9.62\ \mu\text{m}$) and LW9 ($15\ \mu\text{m}$), indicating that the $7.7\ \mu\text{m}$ and $11.3\ \mu\text{m}$ UIB features are present in NGC 7331. The spectrum of the nearby sky is featureless, consistent with the Reach et al. (1996) zodiacal spectrum (Figure 4b). The lack of UIB emission in the off-galaxy positions confirms that the excesses seen in the LW6 and LW8 filters at the galaxy are real and extragalactic, rather than being due to calibration errors or foreground dust. In Figure 4b, 262K and 285K blackbody curves are also shown. The first temperature was found by Reach et al. (1996) for their data, while the latter is the best fit to the COBE DIRBE data for a 3° region centered on NGC 7331, interpolated to the ISO observation date (Reach 1997). The ISO sky fluxes agree with predictions based on the DIRBE data to within 15%.

The total IRAS broadband $12\ \mu\text{m}$ flux density for NGC 7331 is 4.2 Jy (Rice et al. 1988), compared to ~ 2 Jy seen by ISO, so $\sim 1/2$ of the total mid-infrared flux of NGC 7331 is contained within the mapped region. Integrating over the 8 – $15\ \mu\text{m}$ IRAS $12\ \mu\text{m}$ band, the UIBs contribute $\sim 1/3$ of the total IRAS $12\ \mu\text{m}$ flux from NGC 7331.

In Figure 5, the NGC 7331 spectrum is compared to the ISOCAM CVF data for two regions in the Antennae galaxies (from Vigroux et al. 1996): a region containing a powerful starburst (Knot A), and a more quiescent region (the nucleus of NGC 4038). The NGC 7331 spectrum agrees with that for the NGC 4038 nucleus but not the starburst region Knot A. NGC 7331 does not have the steep continuum spectrum seen in starbursts, but rather has a flatter continuum. The difference between the LW3 and LW9 fluxes is probably due to contributions to the broader LW3 filter from the $12.8\text{ }\mu\text{m}$ [Ne II] line, the $12.7\text{ }\mu\text{m}$ UIB, and emission beyond $16.5\text{ }\mu\text{m}$.

Individual spectra for the NGC 7331 ring and a $16''.5 \times 12''.0$ diameter region ($1.2\text{ kpc} \times 0.9\text{ kpc}$) around the bulge are given in Figures 6a and 6b, using an LW3 surface brightness cutoff of 12 MJy sr^{-1} . In Figure 6a the spectrum for the high surface brightness regions ($\text{LW3} \geq 20\text{ MJy sr}^{-1}$) in the ring is also included. In Figure 6c, the spectrum of the lower surface brightness disk is given ($6\text{ MJy sr}^{-1} \leq \text{LW3} \leq 12\text{ MJy sr}^{-1}$). The ring and extended emission each produce $\sim 1/4$ of the total mid-infrared flux from NGC 7331, while the bulge contributes only $\sim 2\%$. The spectrum of the ring is similar to the global spectrum. Furthermore, this spectrum does not change dramatically with a higher or lower surface brightness cutoff (Figures 6a and 6c). This lack of spatial variation in the mid-infrared spectrum has important implications for the nature of the dust emission and its relationship to the optical/UV interstellar radiation field. The UIB features are not significantly weaker in the ring than elsewhere, thus there is no large-scale destruction of the UIB carriers in this region. The comparison with the Antennae galaxy indicates that radiation from the molecule-sized UIB-emitting grains and the larger grains that produce the $15\text{ }\mu\text{m}$ flux are not related to the local star formation rate in the same way; perhaps a stronger and/or harder optical/UV radiation field is needed to excite the grains that produce the $15\text{ }\mu\text{m}$ radiation than the UIB carriers. The UV field in the NGC 7331 ring is not energetic enough to excite much emission from the larger grains that dominate the $15\text{ }\mu\text{m}$ radiation, unlike

in Knot A in the Antennae (Figure 4b). The $15\ \mu\text{m}$ surface brightness in the ring never reaches the levels seen in Knot A ($\leq 30\ \text{MJy sr}^{-1}$ in the NGC 7331 ring vs. $230\ \text{MJy sr}^{-1}$ in Knot A (Tran 1997).

The only place in NGC 7331 where a significant difference in the mid-infrared spectrum is observed is in the bulge, where an excess in the LW2 ($6.75\ \mu\text{m}$) filter is seen, relative to the flux at the other wavelengths (Figure 6b). This short wavelength excess may be due to photospheric light from evolved stars. Assuming that the $2.2\ \mu\text{m}$ light comes from 3000-4000K stars, and scaling the $23''$ aperture K photometry of Aaronson (1977) to the bulge region using the Pogge (1989) red continuum image, interpolation to the mid-infrared shows that most of the emission at $6.75\ \mu\text{m}$ can be accounted for by photospheric emission (Figure 6c). At longer wavelengths, this proportion drops off. At $12\ \mu\text{m}$, roughly half of the observed bulge light may be photospheric. A similar conclusion was reached for the bulge of M31, based on the IRAS data (Soifer et al. 1986). For the ring and diffuse emission, photospheric contributions are negligible.

The detection of the $11.3\ \mu\text{m}$ feature in the bulge, however, indicates that interstellar or circumstellar dust emission is also important in the mid-infrared. Distinguishing between these two possibilities is difficult because the mid-infrared spectra are similar (e.g., Boulanger et al. 1996; Molster et al. 1996). Scaling from the bulge of the Milky Way, Soifer et al. (1986) conclude that in the M31 bulge there are sufficient stars with dust shells to account for the observed IRAS $12\ \mu\text{m}$ emission. This argument may also apply to the bulge of NGC 7331; it has a similar mass and $M/L_{optical}$ ratio as the M31 bulge (Kent 1987), however, its $12\ \mu\text{m}$ luminosity is ~ 3 times higher and its $F_{12\mu\text{m}}/F_{2.2\mu\text{m}}$ ratio is ~ 2 times higher than in the M31 bulge (Soifer et al. 1986), suggesting higher contributions from interstellar dust. On the other hand, NGC 7331 may have a somewhat younger bulge population than M31 (Tosaki & Shioya 1997), affecting the abundance of stars with dust

shells, so this result is uncertain. Further population studies are needed to determine whether there are sufficient dust shell stars in the NGC 7331 bulge to account for the mid-infrared emission.

It is also unclear at present whether sufficient interstellar gas exists in the bulge to account for the observed $11.3\text{ }\mu\text{m}$ emission. The IRAS data imply a total dust mass for NGC 7331 of $2.5 \times 10^7\text{ M}_\odot$ (Young et al. 1989). This is likely a lower limit, since IRAS was not sensitive to very cold dust. Assuming a constant mid- to far-infrared spectrum across the galaxy, the ISO data indicate $M_{dust} \geq 10^5\text{ M}_\odot$ in the bulge, assuming that $\sim 1/2$ of the observed bulge flux is interstellar. Including flux missed by the interferometer and assuming a Galactic I_{CO}/n_{H_2} ratio, the CO map of Tosaki & Shioya (1997) gives an upper limit of $M_{H_2} \leq 9.7 \times 10^7\text{ M}_\odot$ for the bulge. This is sufficient to account for the dust if the gas/dust ratio is ≤ 970 , consistent with typical gas/dust ratios determined from IRAS fluxes (Young et al. 1989). Thus it is possible that sufficient molecular gas is present in the NGC 7331 bulge, but is fainter than current detection limits. In contrast, the HI and H II mass limits appear to be too small to account for this dust. The HI column density in the center of NGC 7331 is $\sim 4\text{ M}_\odot\text{ pc}^{-2}$ (Bosma 1981), implying only $4 \times 10^6\text{ M}_\odot$ of HI in the bulge. From the Pogge (1989) image, $L(H\alpha + [\text{N II}]) \sim 1.3 \times 10^6\text{ L}_\odot$ for the bulge. This flux is mainly [N II], since H α is in absorption (Keel 1983c; Ohyama & Taniguchi 1996). Assuming an absorption-corrected H α /[N II] ratio of 2.5 (Ohyama & Taniguchi 1996), and assuming 10^4 K gas with $n_H \geq 100\text{ cm}^{-3}$ and $A_V \sim 1$ (derived from the dust mass as in Smith & Harvey 1996), $M_{H\text{ II}} \leq 6.0 \times 10^4\text{ M}_\odot$, much too low to account for the dust. Thus, if they are indeed interstellar, the very small grains in the bulge, and the expected larger dust grains that dominate the emission at the longer IRAS bands, are likely associated with molecular gas rather than atomic or ionized gas. More sensitive CO measurements are needed to test this hypothesis.

As noted above, $\sim 1/3$ of the total IRAS 12 μm flux is arising from the UIB features. Although significant, this flux alone is not sufficient to account for the $F(12)/F(60)$ vs. L_{60} trend seen in IRAS broadband colors (Smith et al. 1987; Helou et al. 1991). For moderate luminosity galaxies like NGC 7331, $F(12)/F(60) \sim 0.1$; this ratio decreases by a factor of 3 in high luminosity galaxies (Smith et al. 1987). This implies that, if small grain depletion is responsible for the observed trend in the IRAS colors, the mid-infrared continuum as well as the emission features is affected. Alternatively, other processes may conspire to change the infrared spectrum of galaxies, such as increased 10 μm absorption in high luminosity galaxies or variations in large grain temperatures or properties.

5. Conclusions

ISOCAM imaging of the Sb galaxy NGC 7331 has revealed a bright ring encircling an extended central bulge. The mid-infrared spectrum of NGC 7331 shows one of the first detections of the 7.7 and 11.3 μm dust emission features in a quiescent spiral galaxy. The continuum at 15 μm is weak with respect to the UIB features, in contrast to starburst galaxies, consistent with the moderate L_{FIR} of NGC 7331 and its classification as a relatively quiescent spiral galaxy. Little variation in the mid-infrared spectrum across the galaxy is found with the exception of the bulge, which shows excess 6.75 μm emission, probably caused by photospheric emission. The 11.3 μm feature is also detected in the bulge, however, indicating additional contributions from interstellar or circumstellar dust.

I am grateful to the ISO team for making this project possible. I especially thank the ISOCAM instrument team and the ISO staff at IPAC for their help. This research has made use of the NASA/IPAC Extragalactic Database (NED) which is operated by the Jet Propulsion Laboratory under contract with NASA. This work was supported by ISO data

analysis funding from NASA.

REFERENCES

Aaronson, M. 1977, Ph.D. Thesis, Harvard University

Borghesi, A., Bussoletti, E., & Colangeli, L. 1987, *ApJ*, 314, 422

Bosma, A. 1981, *AJ*, 86, 1791

Boulanger, F., & Perault, M. 1988, *ApJ*, 330, 964

Boulanger, F., et al. 1996, *A&A*, 315, L325

Bronfman, L., Cohen, R. S., Alvarez, H., May, J., & Thaddeus, P. 1988, *ApJ*, 324, 248

Cesarsky, C. et al. 1996, *A&A*, 315, L32

Cowan, J. J., Romanishin, W., & Branch, D. 1994, *ApJ*, 436, L139

Cox, P., Krügel, E., & Mezger, P. G. 1986, *A&A*, 155, 380

de Vaucouleurs, G., de Vaucouleurs, A., Corwin, Jr., H. G., Buta, R. J., Paturel, G., & Fouque, R. 1991, Third Reference Catalogue of Bright Galaxies, Version 3.9

Gautier, T. N., et al. 1984, *ApJ*, 278, L57

Habing, H. J., et al. 1984, *ApJ*, 278, L59

Helou, G., Ryter, C., & Soifer, B. T. 1991, *ApJ*, 376, 505

Helou, G., et al. 1996, *A&A*, 315, L157

Keel, W. C. 1983a, *ApJS*, 52, 229

Keel, W. C. 1983b, *ApJ*, 268, 632

Keel, W. C. 1983c, *ApJ*, 269, 466

Kent, S. M. 1987, AJ, 93, 816

Kessler, M. F., et al. 1996, A&A, 315, L27

Léger, A., & Puget, J. L. 1984, A&A, 137, L5

Molster, F. J. et al. 1996, A&A, 315, L373

Ohyama, Y., & Taniguchi, Y. 1996, in The Physics of LINERS in View of Recent Observations, ASP Conference Series, Vol 103, p. 205

Papoulias, R. et al. 1989, A&A, 217, 204

Pogge, R. W. 1989, ApJS, 71, 433

Reach, W. T. et al. 1996, A&A, 315, L381

Reach, W. T. 1997, private communication

Rice, W., Lonsdale, C. J., Soifer, B. T., Neugebauer, G., Kopan, E. L., Lloyd, L. A., de Jong, T., & Habing, H. J. 1988, ApJS, 68, 91

Roche, P., Aitken, D., Smith, C., & Ward, M. 1991, MNRAS, 248, 606

Sakata, A. et al. 1984, ApJ, 287, L51

Sanders, D. B., Solomon, P. M., & Scoville, N. Z. 1984, ApJ, 276, 182

Sauvage, M. et al. 1996, A&A, 315, L89

Sellgren, K. 1984, ApJ, 277, 623

Siebenmorgen, R., Starck, J. L., Cesarsky, D. A., Guest, S., & Sauvage, M. 1997, ISOCAM Data User's Manual, Version 3.0

Smith, B. J., Kleinmann, S. G., Huchra, J. P., & Low, F. 1987, ApJ, 318, 161

Smith, B. J., & Harvey, P. M. 1996, *ApJ*, 468, 139

Sodroski, T. J., Odegard, N., Arendt, R. G., Dwek, E., Weiland, J. L., Hauser, M. G., & Kelsall, T. 1997, *ApJ*, 480, 173

Soifer, B. T., Rice, W. L, Mould, J. R., Gillett, F. C., Rowan-Robinson, M., & Habing, H. J. 1986, *ApJ*, 304, 651

Starck, J. L., Bijaoui, A., & Murtagh, F. 1995, ‘Multiresolution Support Applied to Image Filtering and Deconvolution”, in CVIP: Graphical Models and Image Processing, Vol. 57, 420

Tosaki, T., & Shioya, Y. 1997, *ApJ*, 484, 664

Tran, D. 1997, private communication

Vigroux, L., et al. 1996, *A&A*, 315, L93

von Linden, S., Reuter, H.-P., Heidt, J., Wielebinski, R., & Pohl, M. 1996, *A&A*, 315, 52

Wegner, G., Haynes, M. P., & Giovanelli, R. 1993, *AJ*, 105, 1251

Young, J. S., Xie, S., Kenney, J. D. P., & Rice, W. L. 1989, *ApJS*, 70, 699

Captions

Fig. 1.— (Plate L1) The Digitized Sky Survey optical image of NGC 7331. The region which was mapped by ISOCAM is outlined. The three small galaxies to the east of NGC 7331 are, south to north, NGC 7337, NGC 7335, and NGC 7336. NGC 7337 and NGC 7335 have redshifts well in excess of that of NGC 7331 (de Vaucouleurs et al. 1991; Wegner, Haynes, & Giovanelli 1993), indicating that they are background galaxies. NGC 7336 has no published velocity. The Digitized Sky Survey, a compressed digital form of the Palomar Observatory Sky Atlas, was produced at the Space Telescope Science Institute under U.S. Government grant NAG W-2166.

Fig. 2.— (Plate L2) The six mosaicked ISO maps of the central region of NGC 7331. For Figures 2a-f, the filters are LW2, LW3, LW6, LW7, LW8, and LW9, respectively. The region mapped by ISO is $5.8' \times 2.25'$. The orientation is marked. Note that the bad ISOCAM column (Cesarsky et al. 1996) is visible at the edges of the mosaicked image, where no overlap is available. For the LW6-9 filters, additional data points are missing because of vignetting at the edges of the array.

Fig. 3.— (Plate L3) The inner region of NGC 7331 at five wavelengths. a) The narrowband 6435\AA continuum image from Pogge (1989). b) The $\text{H}\alpha + [\text{N II}]$ map from Pogge (1989). c) The LW3 map. d) The Pogge (1989) $\text{H}\alpha + [\text{N II}]$ map (contours), superposed on the LW3 map. e) The 20 cm radio continuum map from Cowan et al. (1994) (contours), superposed on the LW3 map. f) The Nobeyama CO (1 – 0) map (Tosaki & Shioya 1997) (contours), superposed on the LW3 map. The field of view of these images is $88'' \times 152''$. North is up and east is to the left. The spatial resolution in the radio continuum and CO maps is $1.8'' \times 1.4''$ and $7.3'' \times 3.7''$, respectively. The primary beam of the Nobeyama array is $65''$; beyond this region the CO map is not reliable. The ISO maps have been aligned using the location of the nucleus on the $\text{H}\alpha + [\text{N II}]$ maps.

Fig. 4.— a). The mid-infrared spectral energy distribution of the mapped region of NGC 7331 (filled triangles). Flux uncertainties of 30% are shown. The horizontal error bars give the wavelength extent of the filters. The six filters are identified. b) The mid-infrared spectrum for the sky near NGC 7331 (filled triangles). The zodiacal spectrum, as measured by the ISOCAM CVF (Reach et al. 1996, revised by Reach 1997), is also plotted (dotted line). The left axis gives the surface brightness scale for the NGC 7331 sky values; the right axis is the scale for the Reach (1997) data. Blackbody curves for 262K and 280K are also displayed (solid and dashed, respectively).

Fig. 5.— The NGC 7331 spectrum, compared with the ISOCAM CVF data for two regions in the Antennae galaxies NGC 4038/4039 (Vigroux et al. 1996, as updated by Tran 1997). The solid line is the spectrum for Knot A, a luminous starburst region, while the dotted line is for the nucleus of NGC 4038. The prominent dust features and the $12.8 \mu\text{m}$ [Ne II] and $15.5 \mu\text{m}$ [Ne III] features are marked.

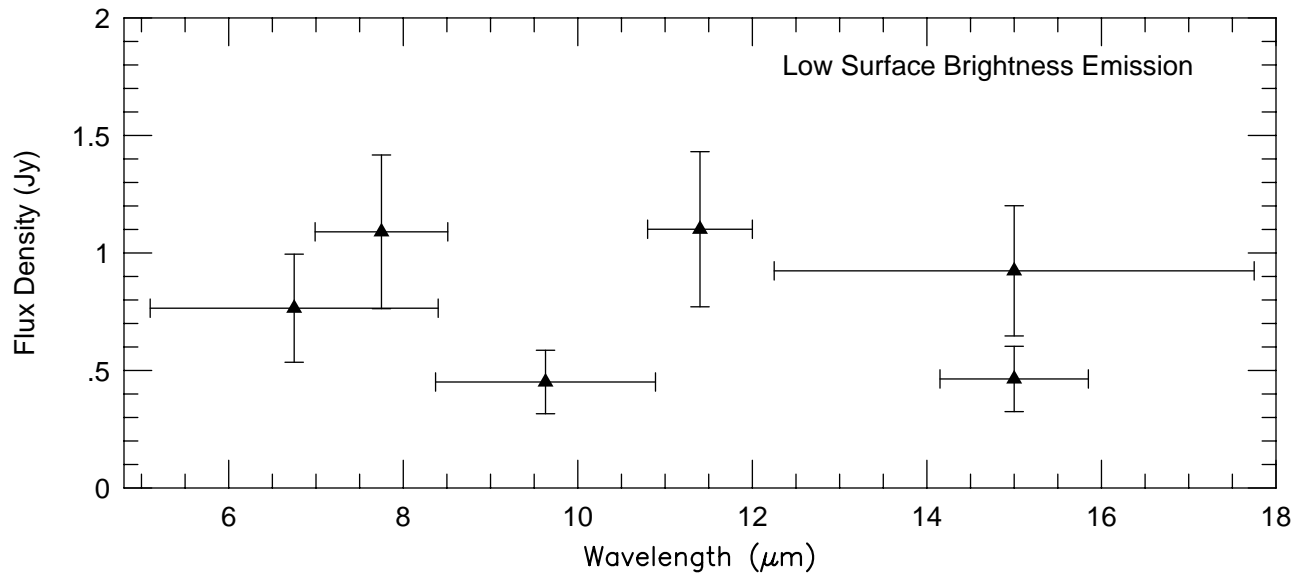
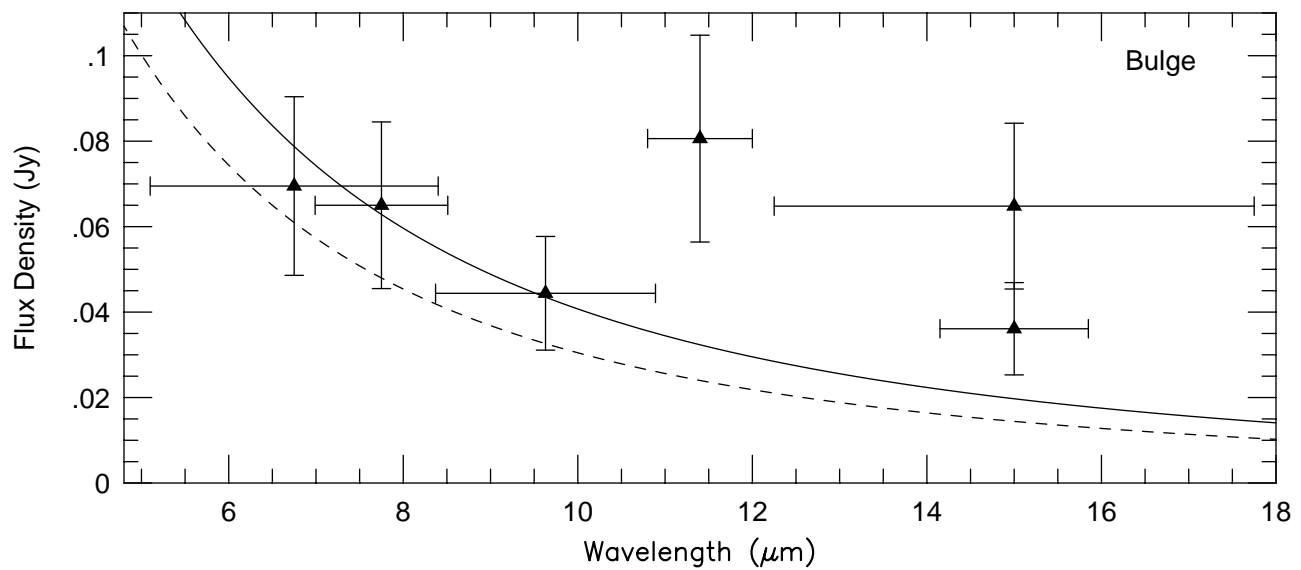
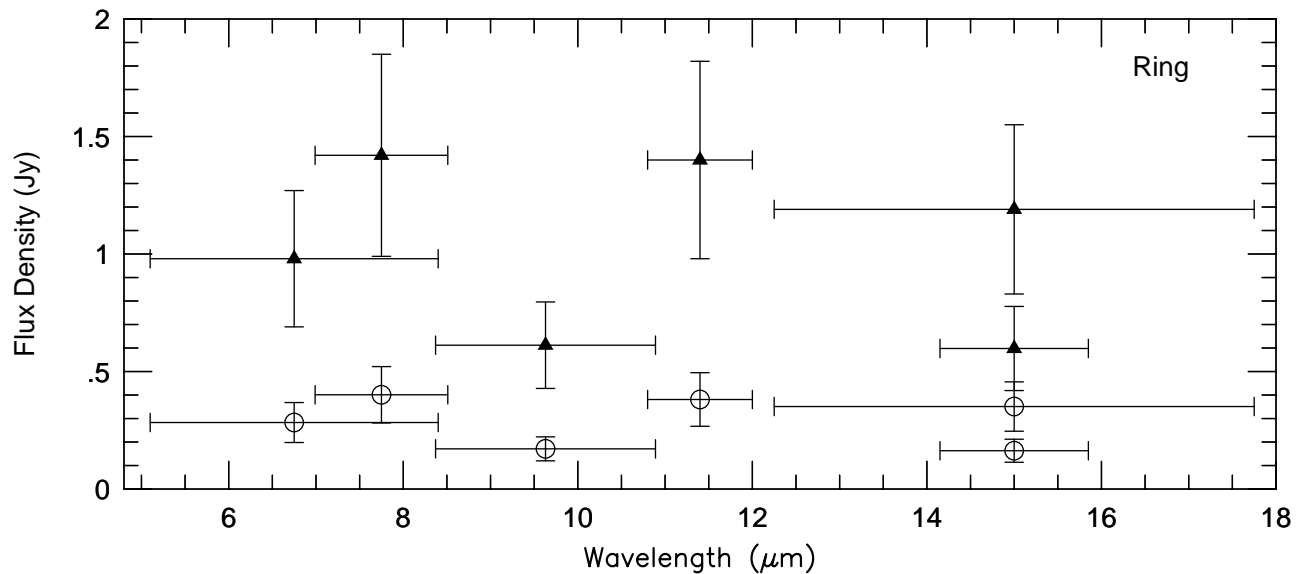
Fig. 6.— The mid-infrared spectrum for a) the NGC 7331 ring, b) the NGC 7331 bulge, and c) the lower surface brightness emission in NGC 7331. In Figures 6a and 6b, data for regions with LW3 surface brightness greater than 12 MJY sr^{-1} are plotted as filled triangles. In Figure 6a, data for regions with LW3 surface brightness greater than 20 MJy sr^{-1} are given as open circles. In Figure 6b, the solid and dashed lines are interpolations from the near-infrared K band flux density for the bulge, assuming blackbody radiation at temperatures of 3000K and 4000K, respectively.

This figure "n7331_fig2_arrow.gif" is available in "gif" format from:

<http://arxiv.org/ps/astro-ph/9801083v1>

This figure "n7331fig3_montage.gif" is available in "gif" format from:

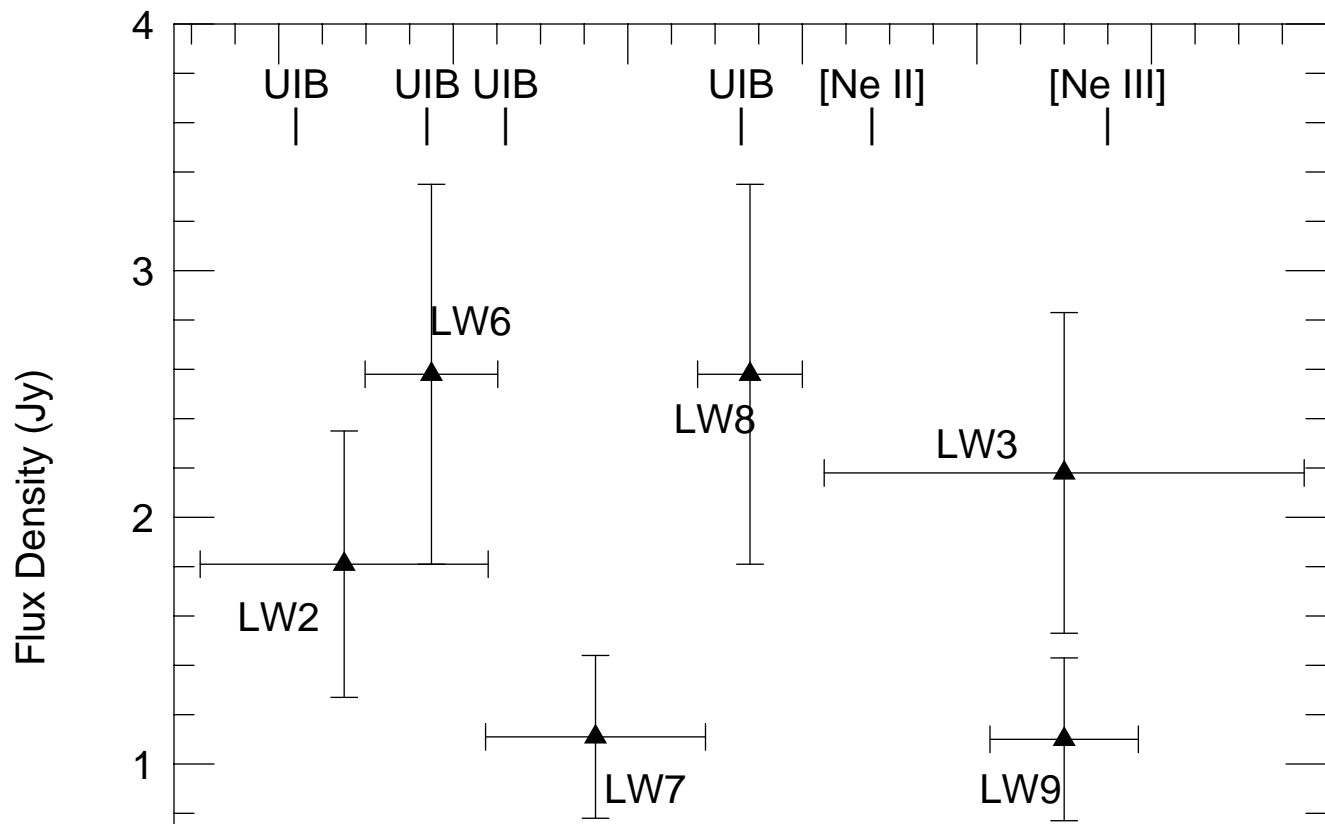
<http://arxiv.org/ps/astro-ph/9801083v1>



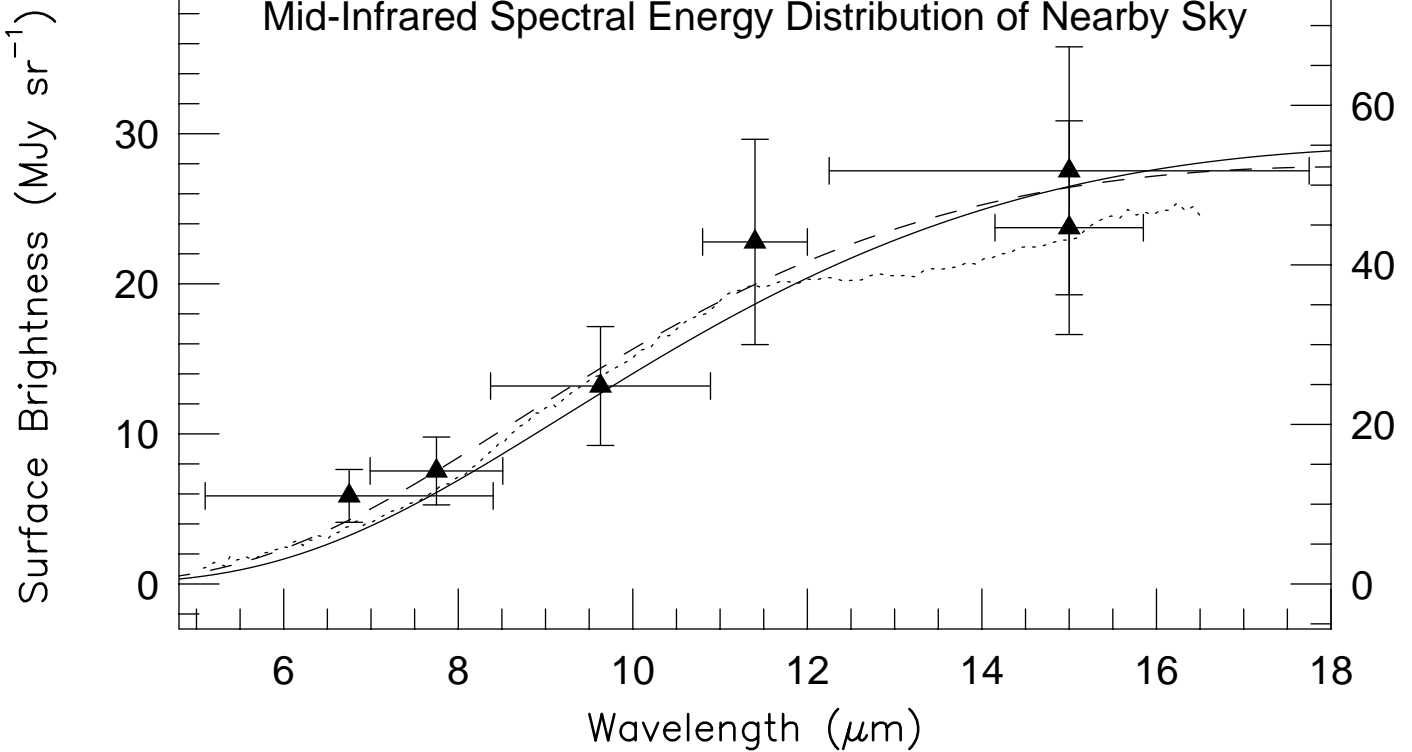
This figure "Fig1_N7331DSS+box.gif" is available in "gif" format from:

<http://arxiv.org/ps/astro-ph/9801083v1>

Mid-Infrared Spectral Energy Distribution of NGC 7331



Mid-Infrared Spectral Energy Distribution of Nearby Sky



NGC 7331 vs. the Antennae

